Computational Analysis of Ares I Roll Control System Jet Interaction Effects on Rolling Moment

Karen A. Deere*, S. Paul Pao†, and Khaled S. Abdol-Hamid‡
NASA Langley Research Center, Hampton, VA, 23681

The computational flow solver USM3D was used to investigate the jet interaction effects from the roll control system on the rolling moment of the Ares I full protuberance configuration at wind tunnel Reynolds numbers. Solutions were computed at freestream Mach numbers from M = 0.5 to M = 5 at the angle of attack 0°, at the angle of attack 3.5° for a roll angle of 120°, and at the angle of attack 7° for roll angles of 120° and 210°. Results indicate that the RoCS housing provided a beneficial jet interaction effect on vehicle rolling moment for M ≥ 0.9. Most of the components downstream of the roll control system housing contributed to jet interaction penalties on vehicle rolling moment.

Nomenclature

A_e	thruster exit area, in.^{2}
alt	altitude, ft
c_{ref}	reference length, based on diameter of first stage core, in.
C_l	rolling moment coefficient = rolling moment / ($q\ S_{ref}\ c_{ref}$)
$C_{l\text{-}TGR}$	rolling moment coefficient – thruster group reference
C_p	pressure coefficient = $(p - p_\infty) / (q\ S_{ref})$
C_{p_firing}	pressure coefficient from the RoCS thrusters firing case
C_{p_idle}	pressure coefficient from the RoCS thrusters idle case
ΔC_p	differential pressure coefficient = $C_{p\_firing} - C_{p\_idle}$
E_J	RoCS jet interaction effects on vehicle rolling moment as percent of thruster-group reference rolling moment, percent, Eq. (4)
$E_{J,\ Component}$	component contribution to jet interaction effects on vehicle rolling moment as percent of thruster-group reference rolling moment, percent, Eq. (5)
f(alt)	factor to account for a varying regulator set point, Eq. (1)
M	Mach number
p	pressure, generic expression, psf
p_e	thruster exit pressure, psf
$p_{e,perfect}$	thruster exit pressure at perfect expansion, psf
$p_{t,j}$	thruster total pressure, psf
p_∞	freestream static pressure, psf
q	dynamic pressure = $\rho V^2 / 2$, psi
S_{ref}	reference area, based on cross-sectional area of core, in.^{2}
T	temperature, generic expression, °R
$T_{mom,e}$	momentum thrust at the thruster exit, lbf
$T_{perfect}$	thrust force at perfect thruster expansion, lbf
T_{vac}	thrust force in vacuum, lbf

* Aerospace Engineer, Configuration Aerodynamics Branch, Research & Technology Directorate, MS 499, AIAA Senior Member
† Aerospace Engineer, Configuration Aerodynamics Branch, Research & Technology Directorate, MS 499, AIAA Associate Fellow
‡ Aerospace Engineer, Configuration Aerodynamics Branch, Research & Technology Directorate, MS 499, AIAA Associate Fellow

T_∞	freestream temperature, °R
u_*	friction velocity at the nearest wall, ft/s
V	freestream velocity, ft/s
x, y, z	Cartesian coordinates, in.
X_p, Y_p, Z_p	missile axes vectors, in.
y_*	distance to the nearest wall, ft
y^+	non-dimensional wall distance for a wall-bounded flow $\equiv \frac{u_* y_*}{\nu}$
α	angle of attack, deg
α_T	total angle of attack in missile axes, deg
β	sideslip angle, deg
γ	gamma, specific heat ratio
η	engine efficiency, Eq. (1)
ν	kinematic viscosity, ft^2/s
ρ	density, $slugs/ft^3$
τ_w	wall shear stress
ϕ	roll angle, deg
ϕ_T	total roll angle in missile axes, deg
$\%_{OR}$	percent over range, convergence Eq. (6)

I. Introduction

Determining the jet interaction effects of the roll control system (RoCS) on the rolling moment of the Ares vehicles is considered very important for guidance, navigation, and control (GN&C) within the Ares I project. This challenging task includes determining how best to model the chemically reactive jet plume from the RoCS and how to capture the plume interactions with the freestream airflow around a vehicle full of protuberances. Jet interaction effects can be measured during experimental tests or computed during investigations with computational fluid dynamics (CFD).

Very few computational investigations have revealed the impacts of installing the RoCS on different configurations. The work of reference 1 investigated the freestream-to-plume interactions on the installed rolling moment for a simplified and smoothed Ares I configuration with a simplified single species gas model of the thrusters, using the Loci/CHEM software. Since the CFD mesh in reference 1 modeled only 180° of the configuration about the vehicle longitudinal axis, variations in the jet interaction effects on rolling moment with vehicle roll angle were not characterized. In reference 2, the authors indicated the importance of modeling the full 360° configuration, which would allow for the possibility of an induced swirl flow around the vehicle. The Ares I-X configuration was used for roll analysis with and without the RoCS activated.[3,4] A full flight-scale mesh of the full protuberance design analysis cycle 2A (DAC2A) geometry was analyzed at many Mach numbers, angles of attack and roll angles with the CFD-FASTRAN software, including a code verification phase prior to computing production runs. The authors of reference 3 applied their roll analysis technique to the RoCS jet interaction effects on the Ares I-X vehicle in a study parallel in time to reference 4, but the results are yet to be archived. Although the computational model for the vehicle and the flow conditions were different from the current work, results presented in reference 4 are valuable cross references to flow physics as seen from a different perspective. For other control jet configurations, such as rocket reaction control system on missiles, a number of recent publications in the open literature reported findings of real gas and ideal gas CFD analysis and some experimental data for validation or comparison.[5-8] Finally, the current authors completed a preliminary computational analysis of the RoCS jet interaction effects on the rolling moment of the Ares I-X simplified configuration.[9] The analysis of reference 9 was used to build confidence in the CFD tools employed in the Ares I project, and for the development of a best practice process for analyzing jet interaction effects from the RoCS thrusters onboard the Ares I vehicle. With no experimental data available and only a few computational works noted above to follow, the best practices established within the Ares project,[10] were used as guidance throughout the computational effort. Certainly, it is ideal to compare computational results with experimental data, but no experimental data was available at the time the computations were needed. A comparison of the results with other computational approaches was the most logical way to check the validity of the computational modeling for RoCS.

The preliminary analysis of the RoCS jet interaction effects on rolling moment of the Ares I-X clean and simplified configuration established a best practice approach of using a USM3D ideal gas analysis with a truncated thruster design to model the RoCS real gas jet plumes.[9] In this modeling approach, the original real gas, convergent-divergent rocket nozzle (fig. 1(a)) is truncated with a plane in the supersonic, divergent section of the nozzle (fig. 1(b)). The convergent section, the nozzle throat region, and part of the divergent section are removed from the real gas thruster nozzle to form the truncated thruster design. The flow originates at the truncation plane using a computed inflow boundary condition that will result in matching five averaged original real gas flow parameters at the exit of the rocket nozzle: density, velocity, mass flow rate, thrust, and static pressure.

Two other approaches to modeling the RoCS thrusters include using real gas simulation in the real thruster geometry or using a boundary condition at the thruster exit plane. First, modeling the full chemical reactions of the rocket plumes, starting at the combustion chamber of the full thruster geometry, was too computationally expensive for this parametric study. For example, the Loci-CHEM solution with the real gas approximation converged in approximately 121 hours (wall time) using 128 processors, or approximately 16000 CPU hours, on a grid size of 29.6 million cells.[9] In contrast, the USM3D ideal gas solution converged in 32 hours using 128 processors, or approximately 4100 CPU hours, on a grid size of 37.4 million cells. Second, using a boundary condition at the thruster exit plane may not allow for flow physics of the jet in cross flow interaction to develop at the exit plane. Therefore, the truncated thruster, with a boundary condition along a face located between the throat and exit plane of the original convergent-divergent thruster design, provides a compromise between these extremes.

In reference 9, the ideal gas thruster modeling in USM3D was compared with a solution using the Loci-CHEM real gas analysis of the full RoCS thruster geometry and with two solutions using OVERFLOW ideal gas analysis applied at the exit of the thrusters. The percent difference between whole vehicle force coefficients of the USM3D ideal gas solution from the Loci-CHEM real gas solution were between 3 and 5 percent, whereas percent difference of whole vehicle rolling moment coefficient between the two codes was 11.6 percent. Qualitatively, the thruster plumes from USM3D and Loci-CHEM solutions compared well. The percent difference of the USM3D (ideal gas truncated nozzle) whole vehicle rolling moment coefficient from OVERFLOW (ideal gas exit boundary condition) was 8.7 percent and 1 percent at Mach 0.9 and 1.6, respectively. The comparisons between different thruster modeling techniques indicated that similar general flow phenomenon around the vehicle were predicted by USM3D, OVERFLOW and Loci-CHEM.

The computational flow solver USM3D was used to investigate the jet interaction effects induced from the roll control system on the Ares I full protuberance configuration. The Ares I configuration used in this report was from Ares I Design and Analysis Cycle (ADAC)–2B, which was conducted on the A103 full protuberances configuration.

All computations in this report used the USM3D code with ideal gas analysis for both external aerodynamics and the RoCS thruster nozzle flow using the above mentioned truncated thruster nozzle model approach. The basic computational grid for the A103 full protuberance geometry was constructed following the best practice for the Ares I project which was developed and refined at each of the ADAC analysis task assignments. The mesh contained 70 million cells. Each of the 12 thrusters were surrounded with approximately 2 million cells to provide adequate grid density to support plume development and jet interactions with the freestream flow. Each solution used at least 6500 CPU hours. The run time for the USM3D code is dependent on grid size and therefore, the larger Ares I protuberance grid required more CPU hours for a converged solution than the smaller Ares I-X mesh.

The investigation included 39 flow conditions, each with idle and firing roll control system thrusters for a total of 78 solutions. A freestream Mach number sweep from M = 0.5 to M = 5 was computed at the angle of attack $\alpha = 0°$, at the angle of attack $\alpha = 3.5°$ for a roll angle of $\phi = 120°$, and at the angle of attack $\alpha = 7°$ for roll angles of $\phi = 120°$ and $\phi = 210°$. The task objective of this investigation was to determine the RoCS jet interaction effects on vehicle rolling moment coefficient C_l. The flow path of the thruster exhaust flow and the plume effect on flow separation over the frustum were investigated.

II. Coordinate System

The reference coordinate systems are shown in figure 2. For USM3D, the positive X axis ($X_{CFD\ Domain}$) must be in the freestream flow direction and the Y ($Y_{CFD\ Domain}$) and Z ($Z_{CFD\ Domain}$) axes aligned in a right handed coordinate system with the X axis. Angle of attack and sideslip angles are specified in the USM3D input file, with angle of attack defined in the X-Z plane and sideslip angle defined in the X-Y plane. Roll angle cannot be specified as a flow variable in the USM3D input file. In order to investigate various roll angles, the vehicle geometry is rotated along with the body axis system in the computational domain. For this study, sideslip angle was specified as zero and body axis angle of attack, α, is equal to the missile axis total angle of attack α_T. Therefore, the α specified within this document is really α_T, but to avoid confusion with the USM3D terminology, α was used throughout this document.

Hence, the computed force and moment coefficients were in the missile axis system for GN&C applications. A conversion from the α_T and ϕ missile axis system can be performed to switch to the α and β body axis system.

Throughout the text, the convention for positive rolling moment was thrusters fired to roll the vehicle clockwise as viewed by the pilot facing forward in the flight direction. Likewise, when a negative roll is discussed throughout the text, the thrusters were fired to generate a negative rolling moment in order to roll the vehicle counterclockwise.

III. Concept Description

Figure 3 shows shaded views of the Ares I A103 configuration rolled at $\phi = 120°$ with several protuberances highlighted in color. The protuberances on this configuration include the upper stage system tunnel (USSTUN), first stage system tunnel (FSSTUN), umbilical, ullage motors, camera pod (CAM), ultra high frequency band antennas (UHF), reaction control system (RCS), stiffener rings (SRings), liquid hydrogen (LH2) feedline, booster deceleration motors (BDM), booster tumbling motors (BTM), and RoCS housing. Reference 11 shows these protuberances on the A103 configuration in detail.

Unlike the Ares I-X configuration in reference 9, the Ares I thrusters in this study are placed symmetrically inside the RoCS housing. There are 12 thrusters total for the Ares I configuration, with 6 thrusters located in the top RoCS and 6 thrusters located in the bottom RoCS housings. In contrast to the thruster 9-inch exit diameter taking up 46 percent of the RoCS housing height on the Ares I-X vehicle, the Ares I thruster exit plane diameter is 3.30 inches or 21 percent of the RoCS housing height. Additionally, the Ares I thrusters are located further away from the vehicle surface by about 5.5 inches and are canted at a 20° angle up from the local tangent to the cylindrical surface to alleviate plume contact with the vehicle's surface.

Figure 4 shows close-up views of the RoCS thruster inflow faces on RoCS housing (blue). There were three thrusters positioned symmetrically on each side of the RoCS housing. At each condition, the firing direction for the thruster-firing CFD computations in this study was chosen based on the sign of the total vehicle aerodynamic rolling moment for the thrusters idle case at that condition. Thus, when the Ares I vehicle was oriented in the missile coordinate system to an angle of $\phi = 90°$ or $\phi = 120°$, the aerodynamic rolling moment was negative with the thrusters idle, so RoCS thrusters 1, 3, 7, and 9 (red and black) were fired together in the thruster-firing CFD simulations to generate a positive rolling moment, to counteract the aerodynamic rolling moment on the vehicle. Similarly, when the Ares I vehicle was oriented in the missile coordinate system to an angle of $\phi = 180°$ or $\phi = 210°$, the aerodynamic rolling moment was positive with the thrusters idle, and RoCS thrusters 4, 6, 10, and 12 (yellow and pink) were fired together to generate a negative rolling moment. The middle thrusters were kept idle at all conditions for this study. The middle thrusters (2, 8, 5, 11) are backup thrusters, used only in case of an emergency, as determined by the program. Follow on studies from this work investigated the use of all three thrusters firing. Since the thrusters are fed from the same manifold pressure, the thrust per engine drops slightly in the case of three thrusters firing, but the total thrust of the three engines is greater than activating only two thrusters.

IV. Methods Description

The NASA Tetrahedral Unstructured Software System (TetrUSS), described in reference 12 and developed at NASA Langley Research Center (LaRC), was used for this computational analysis. TetrUSS includes a model preparation tool (GridTool), grid generation software (VGRID, POSTGRID) and a computational flow solver (USM3D). The USM3D flow solver has internal software to calculate forces and moments. Additionally, the NASA LaRC-developed code USMC6 was used for analyzing the solutions.[13]

A. Grid Generation

The geometry definition was prepared in GridTool.[14] Surface patches were created on the configuration and sources were placed throughout the domain to accurately capture configuration characteristics. The output from GridTool was used to automatically generate the computational domain with the VGRID unstructured grid generation software. VGRID used an Advancing Layers Method to generate thin layers of unstructured tetrahedral cells in the viscous boundary layer,[15] and an Advancing Front Method to populate the volume mesh in an orderly fashion.[16] Finally, POSTGRID was used to close the grid by filling in any gaps that remain from VGRID. POSTGRID is automated to carefully remove a few cells surrounding any gaps in the grid and precisely fill the cavity with the required tetrahedral cells without gaps to finalize the mesh.

The surface shown in figure 3(a) was used to generate the computational domain. The geometry and computational domain were specified in inches. The computational domain extended 6.6 body lengths in the x direction (x = -15847 in. to x = 9729 in.) and extended 8.6 body lengths in the y and z directions (y = -16500 in.

to y = 16500 in. and z = -16500 in. to z = 16500 in.). The unstructured mesh contained 70 million cells. The first cell height in the boundary layer mesh was specified for y^+ values less than one. Average y^+ ranged from $y^+ = 0.2$ for the M = 3 and M = 4 cases, to $y^+ = 0.62$ for the M = 1 cases. The same boundary layer definition was used on all solid surfaces of the configuration, including the inside walls of the thruster. Figure 1(b) shows the mesh inside the truncated thruster, appropriate for ideal gas analysis, used for the current calculations.

B. Computational Flow Solver and Solution Procedure

The TetrUSS flow solver USM3D is a tetrahedral cell-centered, finite volume Euler and Navier-Stokes (N-S) method. The version of the code used for this work was USM3D Version 6.0, updated February 24, 2008 and titled usm3d_60p.altix_sstcompcpd. USM3D has a variety of options for solving the flow equations and several turbulence models for closure of the N-S equations.[12,17] The Spalart-Allmaras (SA) turbulence model was used for all of the flow conditions. The SA turbulence model was implemented with a first order advection term. Prior to this work, the SA turbulence model was typically used for power-off ascent aerodynamics of Ares I configurations.[10] Thus, for consistency in database generation, SA turbulence model was used for the current study.

This study used the implicit Gauss-Seidel scheme and the Roe flux difference-splitting scheme. The code was run in first order spatial accuracy until the residual dropped two orders of magnitude. Then the code automatically switched to generate second order spatially accurate solutions. A typical procedure in this parametric study was to develop each solution for 12000 iterations. If not converged, the solution was continued until the prescribed convergence criteria as described in section F below, were met.

The Mach number, angle of attack, the sideslip angle, and the freestream Reynolds number per unit length specified in millions are specified in the input file for each flow condition. The angle of attack is defined in the X-Z plane and the sideslip angle is defined in the X-Y plane, as shown in figure 2. For this study, sideslip angle is zero ($\beta = 0°$) and thus, body axis angle of attack (α) is equal to the missile axis total angle of attack α_T. The vehicle geometry is rotated along with the body axis system to investigate the effects of roll angle $\phi = \phi_T$.

C. Performance Calculations

A simplified method to calculate thrust performance of a rocket engine is given in reference 18 and summarized here. First, the vacuum thrust performance is calculated by a two-dimensional kinetics method with an engine efficiency parameter, η, and a factor to account for a varying regular set point, f(alt). The actual thrust performance is obtained by subtracting the atmospheric back pressure effect at flight altitude from the vacuum performance:

$$T(alt, A_e) = T_{vac,TDK}(A_e)\eta f(alt) - p_\infty(alt)A_e \tag{1}$$

A common alternate form for thrust performance can be written as:

$$T(alt, A_e) = T_{perfect} - (p_\infty - p_{e,perfect})A_e \tag{2}$$

In the USM3D solution, $T(alt, A_e)$ is represented by the integrated momentum flux and pressure forces at the exhaust plane of the thruster. The effects of total temperature, total pressure, nozzle efficiency, and freestream pressure are automatically taken into account through the N-S method. The computed results, in agreement with Eqs. (1) and (2), do not depend on other parameters such as a freestream Mach number or the spatial orientation of the installed thrusters.

For each iteration, the USM3D code computes the total forces and moments and, if so chosen, the component contributions to the forces and moments and writes them to a file to track the convergence throughout the solution development. The Langley developed post-processing tool, USMC6, is also used to extract data for post-processing and plotting data. USMC6 is instrumental for the calculation of the RoCS thrust. Momentum flux through the inflow plane is added to the pressure coefficient contribution over the inflow plane and over the remainder of the thruster interior surface to compute total thruster thrust. The USMC6 utility is also capable of computing the force and moment coefficients on the basis of individual vehicle components such as thrusters, BTMs or BDMs. In other words, USMC6 can compute all the quantities needed for analysis of the RoCS jet interaction effects in one pass for each flow solution.

There are several equations used to calculate the RoCS jet interaction effects on vehicle rolling moment. First, the thruster-group reference rolling moment $C_{l\text{-}TGR}$ is calculated with Eq. (3) by subtracting the sum of the rolling moments generated by each of the thruster faces in the idle case, from the sum of the rolling moments generated by each of the thruster faces in the thruster-firing case.

$$C_{l-TGR} = \sum_{N=1-8} (C_l)_{FiringCase} - \sum_{N=1-8} (C_l)_{IdleCase} \tag{3}$$

All thruster faces are idle for idle cases. In thruster-firing cases, some of the thrusters are idle and some are firing (1, 3, 7, 9 are fired for a positive rolling moment and 4, 6, 10, 12 are fired for a negative rolling moment). In an effort to account for all of the jet interaction effects, this thruster-group reference rolling moment eliminates very small, but non zero rolling moments in the configuration for the idle case when the RoCS thrusters are all idle, such that only the contributions of the thruster group (firing thrusters) is accounted for in $C_{l\text{-}TGR}$. Second, Eq. (4) is used to calculate E_J, the RoCS jet interaction effects on whole vehicle rolling moment as a percent of $C_{l\text{-}TGR}$.

$$E_J = \frac{\left[(C_l)_{WV\_firing} - (C_l)_{WV\_Idle}\right] - C_{l-TGR}}{C_{l-TGR}} * 100 \tag{4}$$

The term in brackets in Eq. (4) is the difference between whole vehicle rolling moment of the thrusters-firing case $(C_l)_{WV\_firing}$ and the whole vehicle rolling moment of thrusters-idle case $(C_l)_{WV\_idle}$. The thruster-group reference rolling moment $C_{l\text{-}TGR}$ is subtracted from the whole vehicle rolling moment (determined in the bracket) because the whole vehicle term includes the contributions from the thrusters and the desire is know the jet interaction effects on rolling moment from the thrusters without including their direct contribution. The last part to calculating RoCS jet interaction effects on whole vehicle rolling moment E_J with Eq. (4) is to divide the jet interaction effects on rolling moment from the thrusters (without the thruster contribution) by the thruster-group reference rolling moment $C_{l\text{-}TGR}$ and multiply by 100 to get a percentage. Finally, Eq. (5) is used to compute the component contributions of jet effect on rolling moment as a percent of thruster-group reference rolling moment for the RoCS housing, BTM, BDM, FSSTUN, wedges, and the surface not occupied by the protuberances (clean surface).

$$E_{J,Component} = \frac{\left[(C_l)_{Component\_firing} - (C_l)_{Component\_Idle}\right]}{C_{l-TGR}} * 100 \tag{5}$$

The rolling moment of a particular component in the idle case is subtracted from the component rolling moment in the thrusters firing case, and then that quantity is divided by the thruster-group reference rolling moment and multiplied by 100 to get the value as a percentage.

When E_J is positive, there is more rolling moment than expected from the thruster-group reference conditions for a specific altitude, due to beneficial thruster plume interactions on the vehicle components. When E_J is negative, the rolling moment generated is less than expected from the thruster-group reference conditions for a specific altitude because the thruster plume interactions on the vehicle act in the direction opposing the desired roll direction. Throughout the text the term "beneficial" is sometimes used for positive RoCS jet interaction effects on vehicle rolling moment, whereas the term "penalty" is used when E_J is negative. The authors intend for the term "penalty" to simply mean the roll control is less than expected from the RoCS thrusters at a given altitude, whereas the term "benefit" will simply mean the roll control is more than expected from the RoCS thrusters at a given altitude.

D. Initial and Boundary Conditions

A viscous boundary layer condition was used on all solid surfaces. At the truncated inflow faces, an inflow boundary condition was used on the firing RoCS thrusters, whereas an inviscid boundary condition was used on idle thrusters. A supersonic inflow boundary condition was used at the inflow face of the domain and an extrapolation boundary condition was used at the downstream outflow face of the domain. A characteristic inflow and outflow boundary condition was used along the far field, lateral faces of the domain. Complete details for modeling the RoCS thrusters with an ideal gas, truncated nozzle approach are shown in reference 19 under the section heading, Ideal Gas Inflow Equivalence to Real Gas Thruster.

E. Flow Conditions

Solutions were computed at Mach numbers from M = 0.5 to M = 5, for angles of attack $\alpha = 0°$, $\alpha = 3.5°$, and $\alpha = 7°$, and for roll angles of $\phi = 0°$, $\phi = 90°$, $\phi = 120°$, $\phi = 180°$ and $\phi = 210°$ (Table 1). The effects of roll sweep will

not be discussed in this paper, but will be included in reference 20. The conditions were chosen by the program office after (1) negotiations with the customer and the CFD team and (2) evaluating available resources. All calculations were performed at wind tunnel Reynolds numbers.

Table 1. Computational Matrix

Mach	α, °	ϕ, °	RoCS
0.5, 1, 1.2, 1.4, 1.6, 2, 3, 4, 5	3.5	120	Idle, positive
0.5, 0.9, 1, 1.2, 1.4, 1.6, 2, 3, 4	7	120	Idle, positive
0.5, 0.9, 1.2, 1.4, 1.6, 2, 3, 4	7	210	Idle, negative
0.9, 1.6	7	0, 90	Idle, positive
0.9, 1.6	7	180	Idle, negative
0.9, 1.6, 2, 3, 4	0	0	Idle, positive

F. Convergence Criteria

Two main criteria were used to monitor and determine solution convergence. First, a drop in residual (L2-norm of the mean flow residue) of at least three orders of magnitude was desired. Second, convergence of force and moment coefficients was evaluated with a percent over a range ($\%_{OR}$) value of less than 0.5 percent for each coefficient. The $\%_{OR}$ value was calculated with Eq. (6), where C_{Nmax} is the value of the coefficient at the last iteration. The coefficients were averaged over 1000 iterations. The standard deviation and $\%_{OR}$ value were calculated for each coefficient.

$$\%_{OR} = \frac{C_{N_{\max}} - C_{(N_{\max}-999)}}{C_{ave}} \times 100\%$$
$$where: C_{ave} = \frac{1}{1000} \sum_{j=N_{\max}-999}^{N_{\max}} (C_j) \tag{6}$$

G. Computer Platform

All of the solutions were computed at the NASA Advanced Supercomputing (NAS) Columbia system at NASA Ames Research Center. The USM3D flow solver uses approximately 10 μsec/cell/iteration on a single CPU processor. Each solution used 256 processors in parallel to solve the flow equations. Most solutions used 4.8 seconds/cycle/processor.

H. Differential Calculations

The differential pressure coefficient (ΔC_p) is used to illustrate the complexity of jet interaction effects on the overall flow field about the vehicle. The ΔC_p contours were computed by subtracting the surface pressure coefficient of the idle solution (C_{p_idle}), from the RoCS thrusters firing solution (C_{p_firing}), at identical freestream flow conditions. For the ΔC_p plots, green contours represent neutral or no jet interaction effects, blue contours represent decreased pressure and red contours represent increased pressure due to RoCS jet interaction effects. An example of ΔC_p plot is shown in figure 5. In many instances, evaluating differences between the thrusters idle solution and the thrusters firing solution is difficult, compare figure 5(a) with 5(b). However, the jet interaction effects are clearly visible when the differential pressure coefficient is calculated and evaluated, figure 5(c). Differential skin friction analysis was also performed and will be explained in subsection E of section V.

V. Results

The purpose of the roll control system was to maintain vehicle orientation to within 20° of the designed vehicle roll position along the ascent flight path. When initial GN&C simulations did not meet this design criterion,

additional information about the in-flight RoCS performance, to improve control precision, gained in priority.[2] Rocket plumes can induce secondary interactions on the vehicle to reduce or amplify the expected control authority. However, with enough analysis and experimental data, jet interaction effects as a function of Mach number, angle of attack, and vehicle roll angle can be determined. Thus, control uncertainty can be diminished. The current work strives to document the jet interaction effects on vehicle rolling moment induced from the RoCS thrusters on the Ares I A103 configuration. The key components with jet interaction effects on vehicle rolling moment were the two RoCS housings (RoCS), the surface not occupied by protuberances (clean surface), the BTMs, the FSSTUN, the BDMs, and the wedges on the aft skirt.

A. Component Jet Effect versus Mach Number

The E_J parameter, which is a measure of the RoCS jet interaction effects on vehicle rolling moment, is shown in figures 6 through 9 for the whole vehicle and for the key components. The E_J component contributions at $\alpha = 0°$ and $\phi = 0°$ with Mach numbers ranging from M = 0.9 to M = 4.0 are shown in figure 6. The results indicate that the RoCS housing jet effects contributions were beneficial to rolling moment. In addition, E_J for FSSTUN indicates a very small benefit on vehicle rolling moment due the jet interaction effects on the FSSTUN at M = 0.9, M = 1.6, and M = 2.0. All of the other components contributed large jet effect penalties on vehicle rolling moment. In particular, the jet effect penalties on vehicle rolling from the BTM, BDM, and wedges were significantly larger than their corresponding values at $\alpha = 3.5°$ and $\alpha = 7.0°$.

Figures 7 and 8 show the component jet interaction effects for $\alpha = 3.5°$ and $\alpha = 7°$ at $\phi = 120°$, with the RoCS thrusters firing for a positive roll. The Mach number range is expanded in figures 7 and 8 to also include results computed at M = 0.5. Comparisons of E_J component contributions reveal that the overall magnitude of the RoCS housing and clean surface contribution remained about the same as those in figure 6 for $\alpha = 0°$ and $\phi = 0°$. However, the RoCS housing contribution was a penalty at M = 0.5, which was in contrast to all other computed Mach numbers in this report. The jet effect penalty for BTM, BDM, FSSTUN, and wedges diminished with the angle of attack. In fact, some of the components actually showed a jet effect benefit in some cases.

Figure 9 shows the E_J component contributions to the jet interaction effects on rolling moment, for various Mach numbers at $\alpha = 7°$, $\phi = 210°$ and thrusters firing for a negative rolling moment. At both roll angles ($\phi = 120°$ and $\phi = 210°$), the RoCS housing had positive jet interaction effects on rolling moment at all conditions, except M = 0.5. For cases where E_J was near zero, the large benefit from the RoCS housings was depleted by the penalty on the rest of the protuberances downstream of the RoCS housing. The geometry feature that determined if the RoCS housing jet interaction effects were a benefit or penalty to rolling moment was the vertical side faces of the RoCS housing.

B. Whole Vehicle Jet Interaction Results

Figure 10 shows the RoCS jet interaction effects on whole vehicle rolling moment as a function of Mach number for angles of attack of 0, 3.5 and 7 degrees and the thrusters firing to generate a positive rolling moment. The trend in the data shows that the RoCS jet interaction effect on whole vehicle rolling moment was a penalty for most conditions, but that, in general, the penalty decreased as the angle of attack increased. However, a few conditions at higher angles of attack exhibited a jet-induced benefit to rolling moment. At $\alpha = 0°$ and $\phi = 0°$, the RoCS thrusters had a performance deficit of more than 12 percent for all Mach numbers. At $\alpha = 3.5°$ and $\phi = 120°$, the performance deficit was less than 10 percent except at M = 0.5, and there was a benefit to rolling moment at M = 1.4 and M = 1.6. At $\alpha = 7°$ and $\phi = 120°$, E_J was negative for M = 0.5 and M > 1.6, but positive elsewhere with a huge jet-induced benefit to rolling moment at transonic conditions.

An explanation of the trends in figure 10 can be gleaned by considering the component contributions at angles of attack of 0, 3.5, and 7 degrees shown in figures 6, 7, and 8, respectively. Comparisons of figures 6 and 8 show that for M = 1.6 to M = 3, the benefits on the RoCS housings increased as angle of attack increased, whereas the penalty of the wedges, BDMs and clean surface generally decreased, as angle of attack increased from $\alpha = 0°$ to $\alpha = 7°$.

As shown in figure 6, whole vehicle E_J was negative at all Mach numbers at $\alpha = 0°$ and $\phi = 0°$ due to the jet-induced penalties from the wedges, BDM and skin friction on the clean surface. The whole vehicle jet interaction penalty on rolling moment was 12 to 22 percent of the thruster-group reference C_l. Although the jet interaction effects on the RoCS housings were beneficial at all Mach numbers for $\alpha = 0°$, the benefit was eliminated by the penalty on the vehicle's clean surface and the protuberances downstream of the RoCS. In particular, the clean surface, BDMs and wedges had large jet effect penalties on rolling moment. Since the mixed flow would have a direction biased by the plume momentum, flow interactions with the downstream protuberances tend to occur in a direction opposite of the desired direction for roll control. The penalty from the vehicle's clean surface was a result

of skin friction scrubbing the surface in the direction opposing the desired roll direction. The skin friction on the vehicle's surface was substantial, with a penalty of approximately 6 to 9 percent of the thruster-group reference C_l.

The contributions of each component to the jet interaction effects on rolling moment, for Mach sweeps at $\alpha = 3.5°$ and $\alpha = 7°$, are shown in figures 7 and 8, respectively, for the vehicle rolled to $\phi = 120°$ and the thrusters firing for a positive rolling moment. For M = 1.4 at $\alpha = 3.5°$ and $\phi = 120°$, the jet effects contributions of the RoCS housing, BTM, FSSTUN and wedges resulted in small, but positive E_J. At M = 1.6 the large positive contributions of the RoCS housings and wedges resulted in a positive whole vehicle E_J. For M < 1.4 and M > 1.6, the jet-induced penalties on the protuberances far outweighed the jet-induced benefit on the RoCS housings. For M = 0.9 at $\alpha = 7°$ and $\phi = 120°$, the whole vehicle E_J was largely positive due to the 25.38 percent jet-induced contributions from the RoCS housings and 4.74 percent contribution from the FSSTUN (fig. 8).

Figure 11 shows the comparison of the RoCS jet interaction effects on vehicle rolling moment between the configuration rolled to $\phi = 120°$ (thrusters firing for positive roll) and to $\phi = 210°$ (thrusters firing for a negative roll) over the range of Mach numbers at $\alpha = 7°$. The data from each roll angle followed a similar trend over the range of Mach number. At M = 0.9, the jet effect was beneficial for both vehicle roll angles due mostly to the jet-induced forces on the RoCS housings. At M = 0.9, the whole vehicle E_J was larger for the vehicle rolled to $\phi = 120°$ because the contributions from the FSSTUN and BDMs were beneficial (fig. 8), but the contributions from the FSSTUN and BDMs penalized vehicle rolling moment for the vehicle rolled to $\phi = 210°$ (fig. 9). At M = 2, the contribution from the RoCS housings were beneficial for both $\phi = 120°$ and $\phi = 210°$ with about the same magnitude. However, jet interaction effects on vehicle rolling moment, due to the rest of the protuberances, were more detrimental to vehicle rolling moment at a vehicle roll angle of $\phi = 120°$, which eliminated the RoCS housing benefit and resulted in a negative E_J. For the vehicle rolled to an angle of $\phi = 210°$ at M = 2, the jet interaction effects from all of the protuberances (except the wedges) also diminished the jet effect benefit from the RoCS housing, but the whole vehicle jet interaction effect benefit remained positive, near 1.4 percent.

C. RoCS Housings Jet Interaction Effects on C_l

As previously discussed for figure 6 to 9, the dominant components with large jet interaction effects on rolling moment were the RoCS housings. The jet interaction effects were a result of pressure differences on the RoCS housings between the thrusters firing case and the thrusters idle case, for each condition. The main difference between the M = 0.5 and the $M \geq 0.9$ solutions was the suction force on the vertical side face of the RoCS housing that opposed the desired roll direction for M = 0.5. Figure 12 shows the ΔC_p contours on the RoCS housing at several Mach numbers for $\alpha = 7°$ and a vehicle roll angle $\phi = 120°$. For the plots in figure 12, the freestream flows from left to right, the thrusters facing the top of the figure are idle, and the center thruster facing the bottom of the figure is idle. The firing thrusters (1, 3, 7, 9 in figure 4) face the bottom of figure 12, and are positioned to the right and the left of the center idle thruster. The thrusters were firing for a positive rolling moment and had a reaction force in the opposite direction of the plume (not shown).

For M = 0.5, there was a large area of suction force opposing the desired reaction force, as shown by blue contours on the same RoCS vertical side face as the firing thrusters (fig. 12(a)). The extent of the cyan and blue ΔC_p contours on the same side as the firing thrusters extended away from the vertical side face on the vehicle surface. For M = 0.5, the contribution from the RoCS housings was negative ($E_{J\_RoCS} = -8.64$), which meant the jet-induced forces on the RoCS housings opposed and decreased the desired rolling moment. For M = 0.9, the extent of the strong suction on the vehicle surface near the firing thrusters diminished greatly on the bottom RoCS housing, a fair amount on the top RoCS housing, and was replaced with high levels of positive ΔC_p contours (fig. 12(b)), in comparison to M = 0.5. The green contours on the non-firing vertical side face indicate no jet interaction effects. The blue contours on the non-firing vertical side face represent a suction force due to the jets firing, which was not present in the thrusters-idle solution. The combination of large areas of positive ΔC_p on the thrusters firing RoCS vertical side face and the suction on the non-firing thrusters RoCS vertical side face resulted in large jet interaction effects on rolling moment from the RoCS housings ($E_{J\_RoCS} = 25.38$) in the desired roll direction. The extra push on the RoCS housings and the positive jet-induced force on the FSSTUN resulted in a 28 percent larger whole vehicle rolling moment than expected, compared to the thruster-group reference C_l (fig. 8).

For the supersonic cases in figure 12, the non-firing vertical side face of the RoCS housings saw little change from the idle solution to the firing solution, as represented by green ΔC_p contours. For the M = 1.2 case (fig. 12(c)), the firing thruster vertical side face had large areas of positive ΔC_p in front of each firing thruster and a smaller area of suction behind each thruster, with a net positive jet interaction effect on rolling moment from the RoCS housings. For the M = 2 case (fig. 12(d)), the suction behind each thruster on the bottom RoCS housing diminished, which

increased the net positive jet interaction effect on rolling moment due to the RoCS housings in comparison to the M = 1.2 case. By M = 4 (fig. 12(e)), the jet interaction effects on rolling moment due to the RoCS housings diminished in comparison to the other cases as represented by mostly green contours of ΔC_p. There was a small jet-induced benefit (E_{J_RoCS} = 3.15 percent) at M = 4 from increased pressure in front of the firing thrusters.

D. BTM Jet Interaction Effects on C_l

There were only three conditions of all the cases analyzed in which the BTM contribution to rolling moment produced a benefit of more than 1 percent of the thruster-group reference $C_{l\text{-}TGR}$, as shown by a comparison of the purple bars for the BTM in figures 6 to 9. All three cases occurred below Mach 1.6, at $\alpha = 3.5°$, $\phi = 120°$, and with the thrusters firing for a positive rolling moment. Figure 13 illustrates the differences between a positive and negative contribution to rolling moment from jet-induced forces on the BTM. The comparison of differential pressure coefficient between the M = 1.0 and M = 1.2 solutions, both with $\alpha = 3.5°$, $\phi = 120°$, and with the thrusters firing for a positive rolling moment is shown in figure 13. Red ΔC_p contours indicate increased pressure on the surface when the thrusters were firing, in comparison to the thrusters-idle solution. For the M = 1.0 solution, ΔC_p contours were neutral green on the BTM vertical side facing the RoCS housing and were cyan on the opposite vertical side face (suction opposing roll direction), which resulted in a negative rolling moment and a jet interaction effect from the BTM of E_J = -3.99 percent. In contrast for the M = 1.2 solution, ΔC_p contours were mostly blue on the BTM vertical side facing the RoCS housing (strong suction in desired roll direction) and were red on the opposite BTM vertical side face (push in desired roll direction), which resulted in a positive rolling moment and a BTM E_J = 8 percent. The effects of a bow shock at the RoCS housing is shown with red ΔC_p contours at both Mach numbers. There was also a bow shock affecting the BTM for the M = 1.2 solution, that was not present in the M = 1.0 solution. The jet effect on the BTM bow shock at M = 1.2 was to pressurize the vertical side face in favor of the desired rolling moment.

E. First Stage Jet Interaction Effects on C_l

The differential skin friction coefficient vector lines shown in figures 14 to 16 represent changes in skin friction vector directions from that of the RoCS thrusters idle solution to that of the RoCS thrusters firing solution. It should be noted that the differential skin friction coefficient vector calculation represents a change in the skin friction force vector from the thrusters idle solution to the thrusters firing solution. When the differential skin friction vector line points in a direction opposing the freestream, it signifies a reduction in the axial skin friction force, and does not necessarily indicate flow reversal.

The differential pressure coefficient contours and differential skin friction coefficient vector lines shown in figures 14 to 16 illustrate the complexity of jet interaction effects on the overall flow field about the surface of the vehicle. These figures for M = 1.2, M = 1.6, and M = 3 show changes in skin friction coefficient vector in response to the changes in local flow directions between the RoCS firing and non-firing solutions near the vehicle body. The changes were a result of jet mixing, as the RoCS jet plumes entrained air flow from the non-firing side of the RoCS housing and pulled the flow in the direction of the jet plume trajectory. This kinematic flow feature persisted downstream of the RoCS housing, by which point the original plume trajectory had been deflected by freestream interactions.

The BDMs are located on the aft skirt as shown in figure 3(c). The jet interaction effect on the BDM (or any component) was the integrated pressure change from the idle solution to the thrusters-firing solution. Regions of no jet interaction effects appear as green contours. Jet interaction effects on rolling moment occurred when the integrated pressure change resulted in a net force acting to increase or decrease rolling moment. In figure 14 for M = 1.2, there were large positive and negative pressure differentials on the BDMs and the penalty on rolling moment due to the BDMs was -9.25 percent (fig. 7). In figure 15 for M = 1.6, the pressure differentials on the BDMs were less severe and the penalty on rolling moment from jet interaction effects due to the BDMs decreased to nearly -3 percent. In figure 16 for M = 3, the negative pressure differential on some of the BDMs was less severe than at M = 1.2, but covered more area than at M = 1.6, which resulted in a 5.7 percent penalty on rolling moment due to jet interaction effects on the BDMs for M = 3. It is also worth noting that the pressure changes on the vehicle were the strongest on and near the RoCS housing. As seen in the top grey box of each figure, the RoCS vertical side face had a large area of red ΔC_p contours, which acted in the direction of the desired rolling moment and resulted in large positive jet interaction effects from the RoCS housing at all three Mach numbers (fig. 7). Furthermore, jet interaction effects were mostly absent upstream of the RoCS housing due to the nature of a supersonic freestream.

VI. Conclusions

This computational investigation examined the jet interaction effects of the roll control system (RoCS) on rolling moment of the Ares I full protuberance vehicle. Computational solutions were computed with USM3D for a broad range of flow conditions ranging in Mach numbers from 0.5 to 5.0, at three angles of attack (0°, 3.5°, 7°) and three roll angles (0°, 120°, 210°). All calculations were performed at wind tunnel Reynolds numbers.

Some general observations from the detailed analysis of the itemized component contributions to jet interaction effects on rolling moment include the following. First, the largest and mostly positive contributor to thruster efficiency was the jet-induced pressure on the RoCS housings. Second, the contribution from the clean surface was always a penalty, due to the skin friction force over the clean surface acting in a direction contrary to the intended roll control action. Third, with a few exceptions, the jet interaction effects on the BDMs resulted in large penalties to rolling moment. Finally, the jet effect contributions from the wedges were mostly very small, except at $\alpha = 0°$. Nevertheless, these observations do not shed much light on the complexity of the total jet effect as a function of Mach number, α and ϕ.

In more detail, the jet-induced penalty on rolling moment for the Mach number sweep at $\alpha = 0°$ and $\phi = 0°$ was 12 to 22 percent of the thruster-group reference C_l. If only the pressure footprint on the RoCS housing was considered, the jet interaction effects on rolling moment was substantially beneficial. However, the vehicle clean surface, BDMs, and wedges all had large negative contributions to rolling moment due to jet interaction effects from the RoCS thrusters firing. The 5 to 9 percent penalty to rolling moment from the vehicle's clean surface was a result of skin friction scrubbing the surface in the direction opposing the desired roll direction.

An analysis of the component-by-component contributions to rolling moment from the RoCS jet interaction effects on the components indicated that the skin friction acting on the clean surface of the vehicle always acted in the direction opposing the desired rolling moment, independent of Mach number, angle of attack or vehicle roll angle. The clean surface detrimental contribution ranged from $E_J = -0.71$ percent to as high as $E_J = -9.18$ percent. In contrast, the RoCS housing always provided a jet-induced benefit to rolling moment with positive values of E_J for $M \geq 0.9$, at all angles of attack and vehicle roll angles.

Finally, an analysis of the component-by-component contributions to rolling moment as a result of the RoCS jet interaction effects indicated that the sum of the pressure footprint on the RoCS housing and the protuberances downstream of the RoCS installation, along with skin friction on the vehicle surface, accounted for all of the jet interaction effects on rolling moment.

References

[1]Morris, C. I., "Ares I FS RoCS Installed Roll Performance Analysis," RCS-RPT-Analysis-098. March 25, 2008.

[2]Ruf, J. H., and Morris, C. I., "Results of ER43 Second Cycle of Analysis on CLV First Stage Roll Control Thruster Effects," Memo number ER43 (06-018), October 23, 2006.

[3]Meyer, B., Slaby, M., and Habchi, S., "Ares I-X CFD Roll Analysis," MSFC Contractor's Report, Jacobs Task Order no. 45-010003-CG, CFDRC Project no. 8845, CFD Research Corporation, Huntsville, AL, December 2007.

[4]Daley, P., Meyer, B., Slaby, M., Sheta, E., and Habchi, S., "Ares I-X Roll Control System Plume Effects on Forces and Moments," CFDRC Report Number 8845-01, September 2008.

[5]Gnemmi, P., and Schafer, H-J., "Experimental and Numerical Investigations of a Transverse Jet Interaction on a Missile Body," AIAA 2005-52, January 10-13, 2005.

[6]Ebrahimi, H. B., "Numerical Investigation of Jet Interaction in a Supersonic Freestream," J. Spacecraft and Rockets, vol. 45, no.1, pp-95-103, February 2008.

[7]Graham, M. J., Weinacht, P., Brandeis, J., and Angelini, R., "A Numerical Investigation of Supersonic Jet Interaction for Finned Bodies," Army Research laboratory Report ARL-TR-2312, Aberdeen Proving Ground, MD, December 2000.

[8]Seiler, F., Gnemmi, P., Ende, H., and Schwenzer, M., "Jet Interaction at Supersonic Cross Flow Conditions," Shock Waves, vol. 12, pp. 13-23, 2003.

[9]Deere, K. A., Pao, S. P., and Abdol-Hamid, K. S., "A Computational Investigation of the Roll Control System Jet Interactions on Rolling Moment of the Simplified Ares I-X Configuration," NASA TP (submitted for publication).

[10]Pao, S. P., Vatsa, V. N., Abdol-Hamid, K. S., Pirzadeh, S., Samareh, J. A., Klopfer, G. H., Taft, J. R., and Parlette, E. B., "Best Practice for Ascent Aerodynamics Analysis for the Ares I Configurations," Special Session at 55th JANNAF Propulsion Meeting in Boston, MA, May 12-16, 2008.

[11]Abdol-Hamid, K. S., Ghaffari, F., Pao, S. P., Deere, K. A., Elmiligui, A., and Parlette, E. B., "Computed Turbulent Ascent Aerodynamic Data Analysis for the Proposed Ares I ADAC–2B (A103) Configuration," Ares–AD–TA–0012, version 1.0, May 2008.

[12]Frink, N. T., Pirzadeh, S. Z., Parikh, P. C., Pandya, M. J., and Bhat, M. K., "The NASA Tetrahedral Unstructured Software System," The Aeronautical Journal, Vol. 104, No. 1040, pp. 491–499, October 2000.

[13]Pao, S. P., "USMC6-TetrUSS Grid and Solution Cutter: A Brief Users' Guide," Version 4, NASA Langley Research Center, October 2008.

[14]Samareh, J., "GridTool: A Surface Modeling and Grid Generation Tool," Proceedings of the Workshop on Surface Modeling, Grid Generation, and Related Issues in CFD Solutions, NASA CP–3291, May 9–11, 1995.

[15]Pirzadeh, S., "Unstructured Viscous Grid Generation by Advancing-Layers Method," AIAA Journal, Vol. 32, No. 8, pp. 1735–1737, August 1994.

[16]Pirzadeh, S., "Structured Background Grids for Generation of Unstructured Grids by Advancing Front Method," AIAA Journal, Vol. 31, No. 2, pp. 257–265, February 1993.

[17]Pandya, M. J., Abdol-Hamid, K. S., and Frink, N. T., "Enhancement of USM3D Unstructured Flow Solver for High-Speed High-Temperature Shear Flows," AIAA 2009-1329, The 47th AIAA Aerospace Sciences Meeting, January 5-8, 2009.

[18]Pasch, J., "Ares 1-X Roll Control System Thrust Prediction Methodology," Contract NNM05AB50C, Task Order 33–020302–CC, January 11, 2008.

[19]Pao, S. P., Deere, K. A., and Abdol-Hamid, K. S., "Establishing Approaches for Modeling Ares Roll Control System With Ideal Gas Truncated Nozzles," 49th AIAA Aerospace Sciences Meeting, American Institute of Aeronautics and Astronautics, Reston, VA, January 2011 (submitted for publication).

[20]Deere, K. A., Pao, S. P., and Abdol-Hamid, K. S., "A Computational Investigation of the Roll Control System Jet Interaction Effects on Rolling Moment of the Ares I Full Protuberance Configuration," NASA TP (submitted for publication).

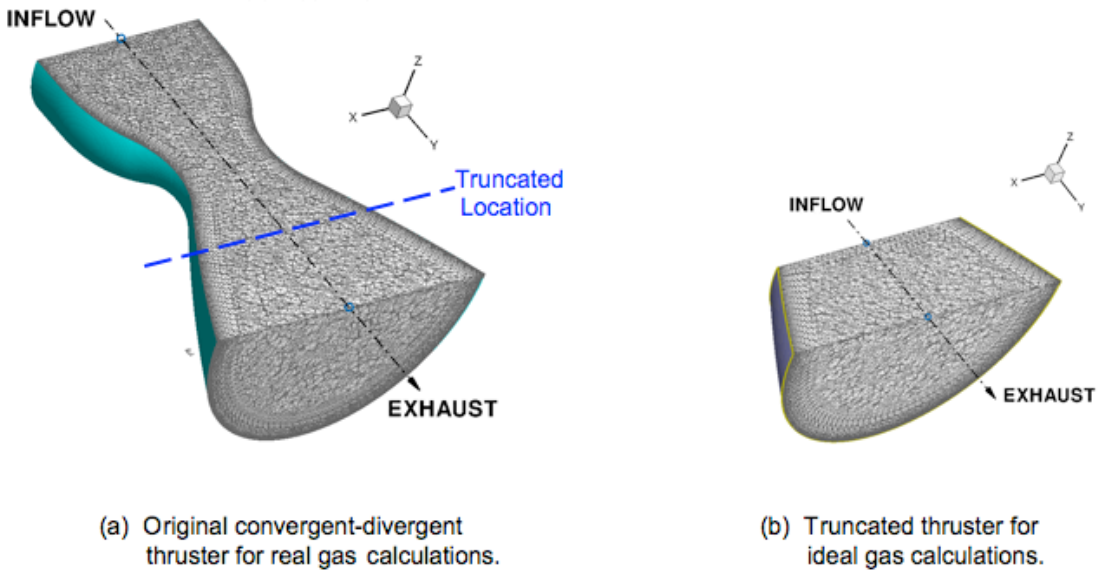

(a) Original convergent-divergent thruster for real gas calculations.

(b) Truncated thruster for ideal gas calculations.

Figure 1. Two methods for modeling the RoCS thruster geometry.

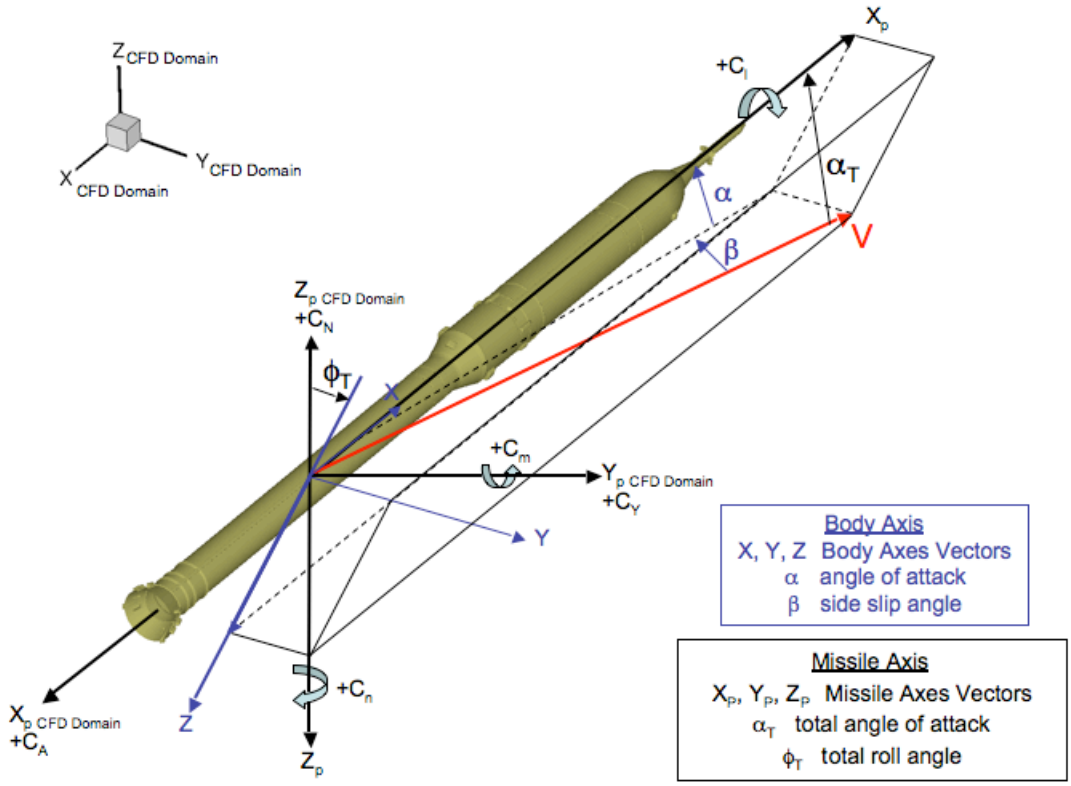

Figure 2. Reference coordinate systems.

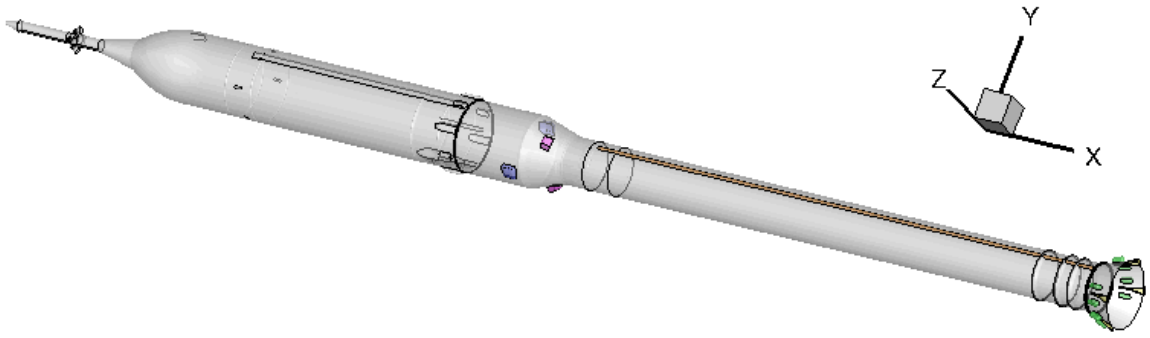

(a) Full configuration.

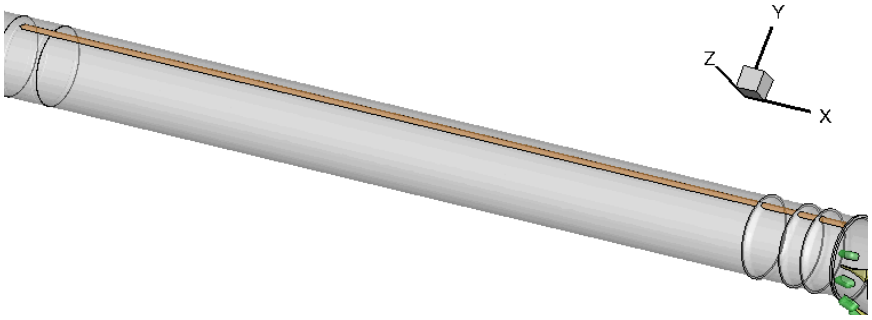

(b) First stage system tunnel shaded orange.

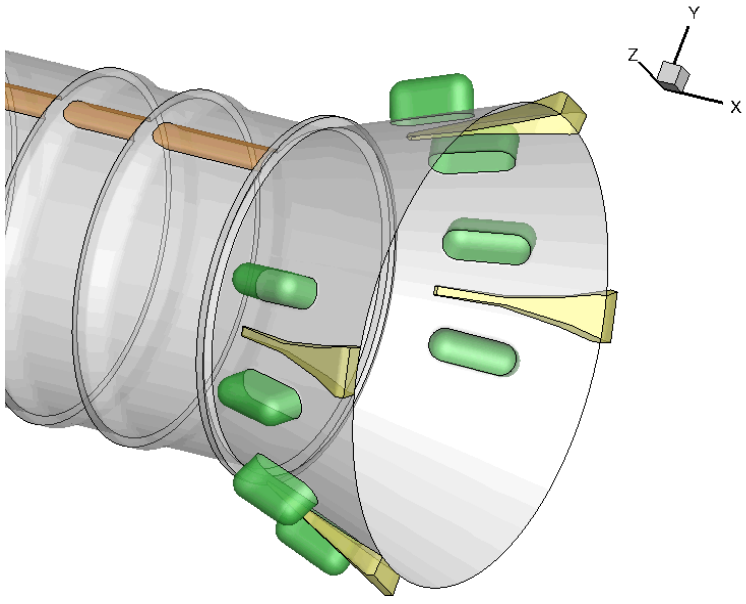

(c) BDMs shaded green and wedges shaded yellow.

Figure 3. Computational surface for the Ares I full protuberance configuration.

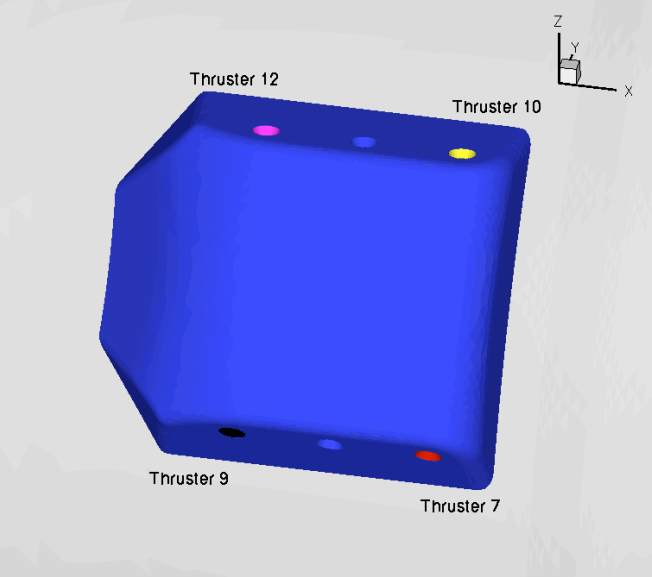

(a) Top RoCS housing.

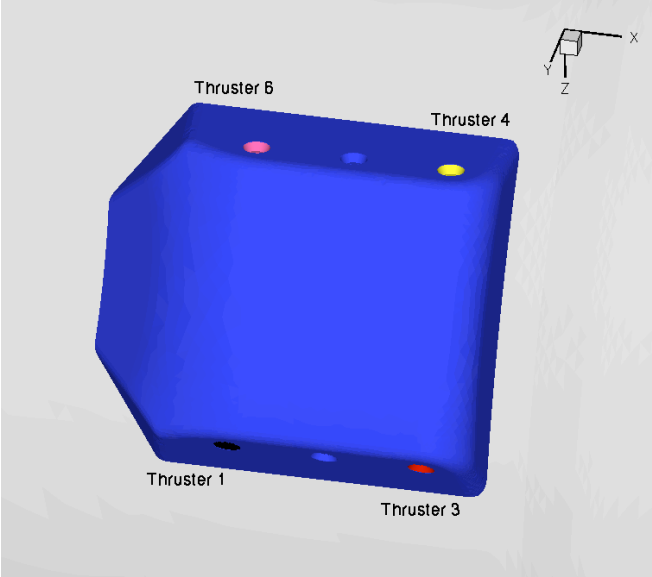

(b) Bottom RoCS housing.

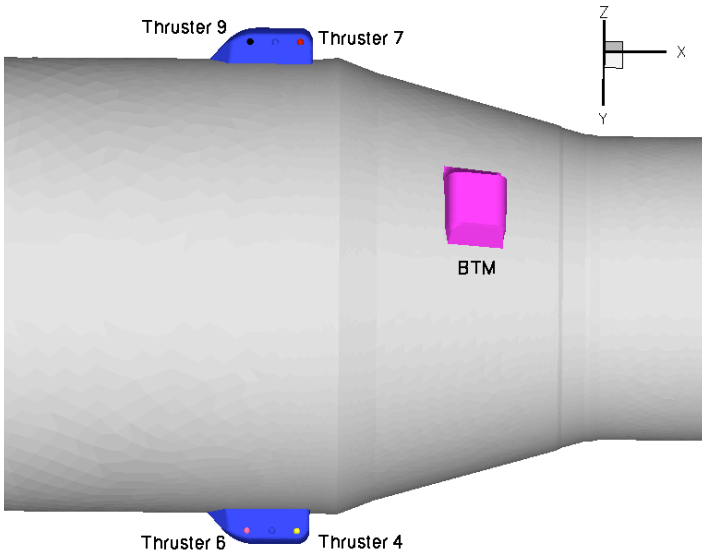

(c) Sideview of the Top and Bottom RoCS housings, the frustum, and one BTM.

Figure 4. Symmetric alignment of the thruster inflow faces in the RoCS housing (blue). Thrusters 1, 3, 7 and 9 are fired for positive rolling moments and Thrusters 4, 6, 10 and 12 are fired for negative rolling moments.

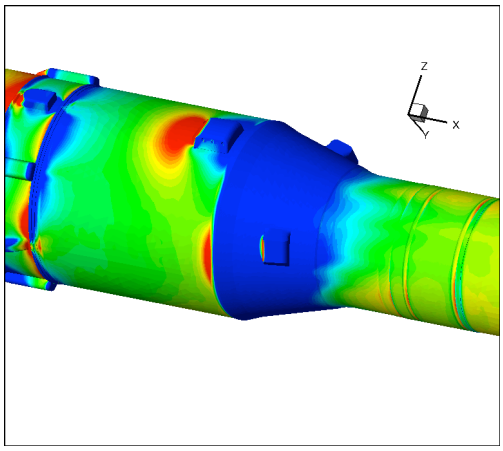

(a) Pressure coefficient for the idle case.

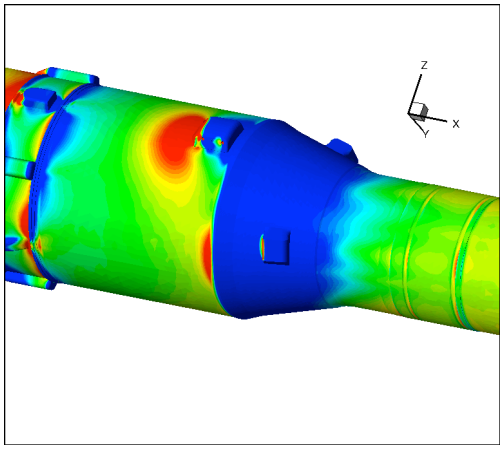

(b) Pressure coefficient for the thrusters firing case.

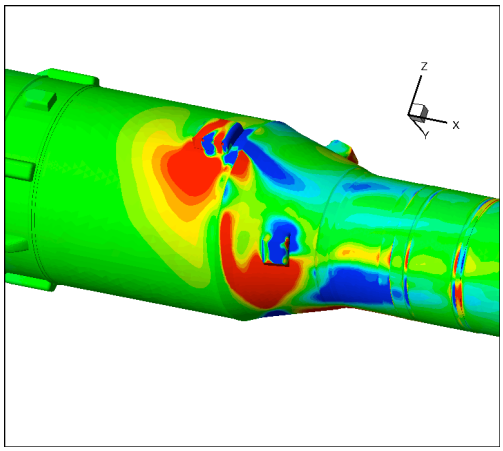

(c) Differential pressure coefficient.

Figure 5. Comparison of pressure coefficient contours to differential pressure coefficient contours for M = 1.2, α = 3.5°, ϕ = 120°.

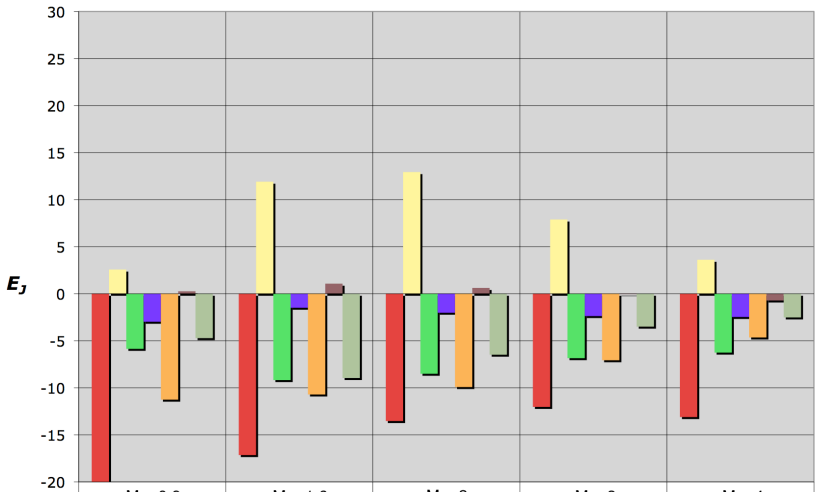

	M = 0.9	M = 1.6	M = 2	M = 3	M = 4
WV	-22.00	-17.15	-13.53	-12.03	-13.11
RoCS	2.57	11.91	12.93	7.89	3.61
clean surface	-5.86	-9.18	-8.51	-6.85	-6.26
BTM	-2.98	-1.49	-2.02	-2.37	-2.47
BDM	-11.26	-10.71	-9.92	-7.07	-4.65
FSSTUN	0.26	1.07	0.62	0.01	-0.72
wedges	-4.72	-8.96	-6.48	-3.50	-2.52

Figure 6. Jet interaction contribution from each component for α = 0°, ϕ = 0°, and thrusters firing for a positive rolling moment.

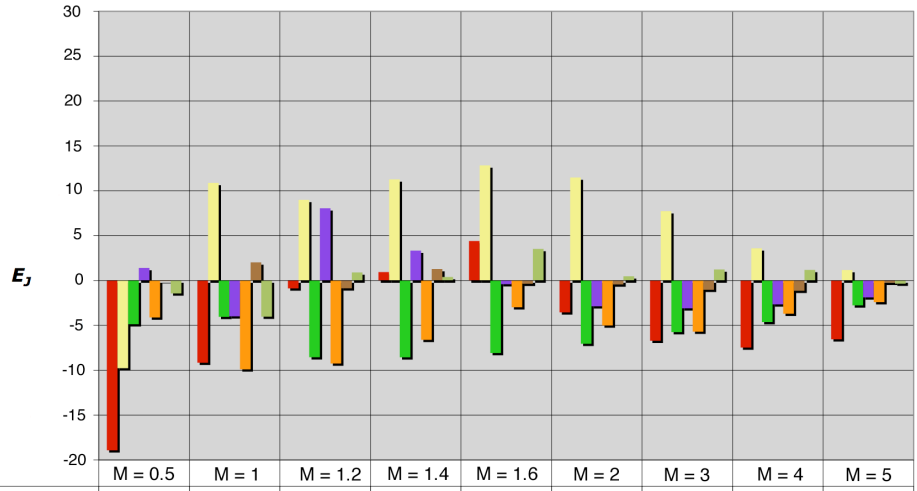

	M = 0.5	M = 1	M = 1.2	M = 1.4	M = 1.6	M = 2	M = 3	M = 4	M = 5
WV	-18.92	-9.16	-0.88	0.94	4.40	-3.55	-6.71	-7.47	-6.55
RoCS	-9.77	10.88	8.99	11.27	12.83	11.48	7.73	3.59	1.17
clean surface	-4.87	-4.05	-8.55	-8.56	-8.08	-7.05	-5.75	-4.63	-2.77
BTM	1.40	-3.99	8.05	3.33	-0.41	-2.87	-3.10	-2.66	-1.88
BDM	-4.12	-9.90	-9.25	-6.61	-2.98	-5.01	-5.70	-3.70	-2.41
FSSTUN	-0.02	2.02	-0.87	1.28	-0.36	-0.44	-1.03	-1.14	-0.25
wedges	-1.44	-4.03	0.90	0.39	3.52	0.47	1.23	1.18	-0.35

Figure 7. Jet interaction contribution from each component for α = 3.5°, ϕ = 120°, and thrusters firing for a positive rolling moment.

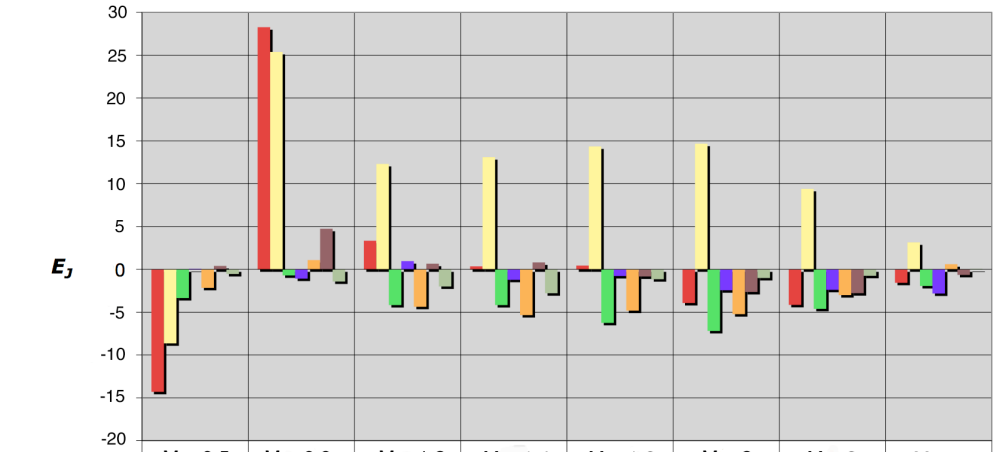

	M = 0.5	M = 0.9	M = 1.2	M = 1.4	M = 1.6	M = 2	M = 3	M = 4
WV	-14.30	28.27	3.34	0.35	0.44	-3.93	-4.15	-1.57
RoCS	-8.64	25.38	12.31	13.10	14.35	14.67	9.40	3.15
clean surface	-3.35	-0.71	-4.17	-4.17	-6.25	-7.19	-4.61	-1.94
BTM	0.05	-1.08	0.96	-1.22	-0.78	-2.44	-2.39	-2.82
BDM	-2.16	1.08	-4.37	-5.34	-4.82	-5.23	-3.01	0.60
FSSTUN	0.40	4.74	0.66	0.81	-0.83	-2.64	-2.78	-0.65
wedges	-0.54	-1.42	-2.00	-2.79	-1.15	-1.01	-0.75	0.06

Figure 8. Jet interaction contribution from each component for α = 7°, ϕ = 120°, and thrusters firing for a positive rolling moment.

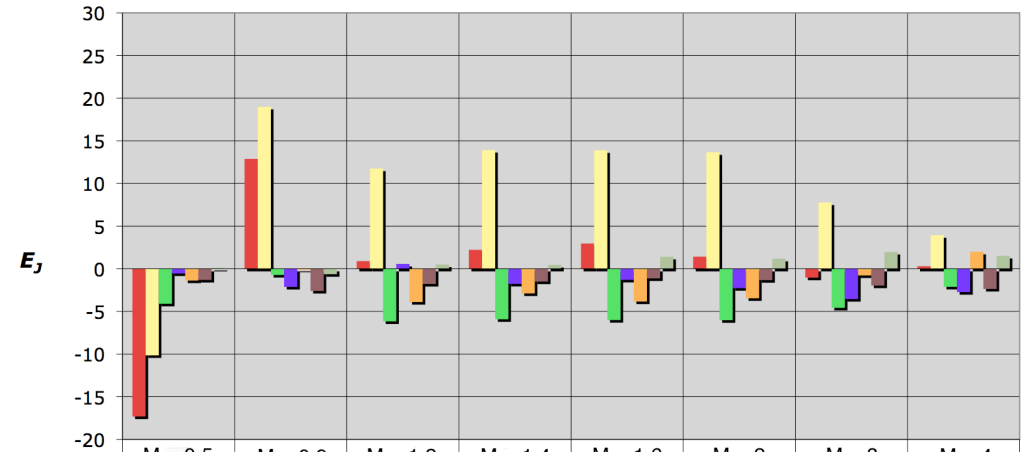

	M = 0.5	M = 0.9	M = 1.2	M = 1.4	M = 1.6	M = 2	M = 3	M = 4
WV	-17.32	12.88	0.90	2.22	2.96	1.42	-1.04	0.30
RoCS	-10.15	18.99	11.76	13.93	13.89	13.66	7.78	3.94
clean surface	-4.10	-0.73	-6.17	-5.92	-6.01	-6.03	-4.58	-2.12
BTM	-0.55	-2.13	0.57	-1.77	-1.30	-2.27	-3.55	-2.74
BDM	-1.38	-0.11	-3.90	-2.89	-3.84	-3.46	-0.78	2.00
FSSTUN	-1.31	-2.60	-1.78	-1.50	-1.13	-1.33	-1.97	-2.36
wedges	0.11	-0.63	0.50	0.45	1.41	1.18	1.98	1.52

Figure 9. Jet interaction contribution from each component for α = 7°, ϕ = 210°, and thrusters firing for a negative rolling moment.

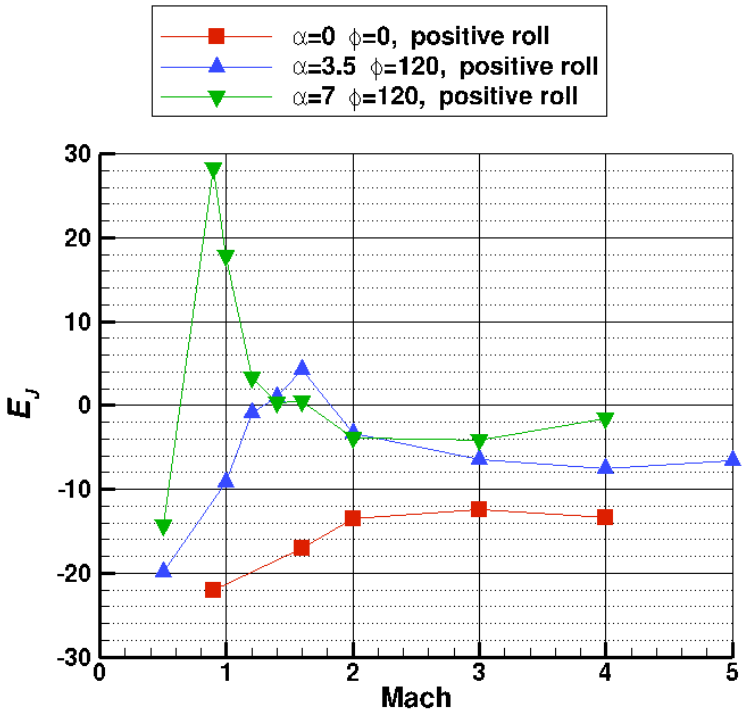

Figure 10. Whole vehicle jet interaction effects on vehicle rolling moment as a function of Mach number and angle of attack.

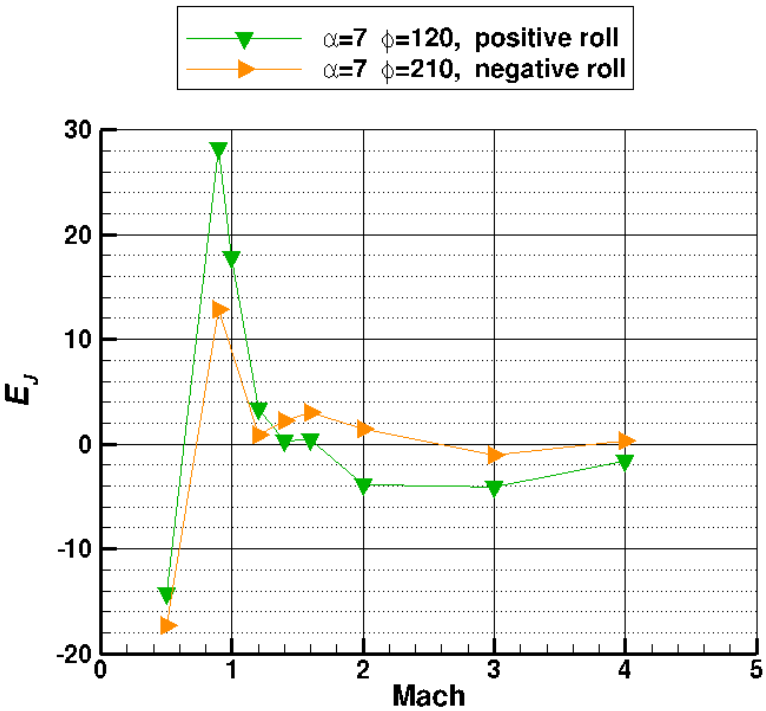

Figure 11. Whole vehicle jet interaction effects on rolling moment for α = 7°. A comparison between the configuration rolled to ϕ = 120° and to ϕ = 210°.

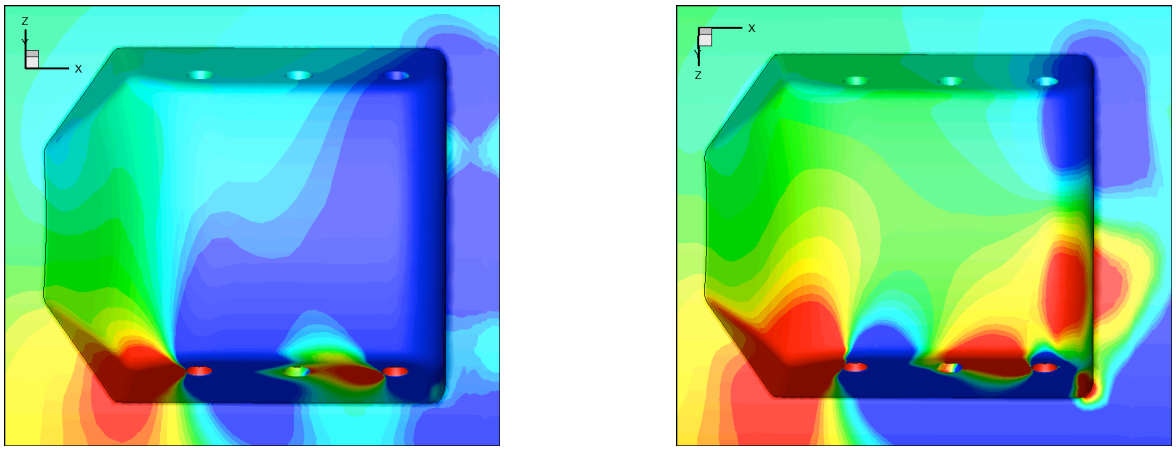

(a) Mach 0.5, E_{J_WV} = -14.30, E_{J_RoCS} = -8.64.

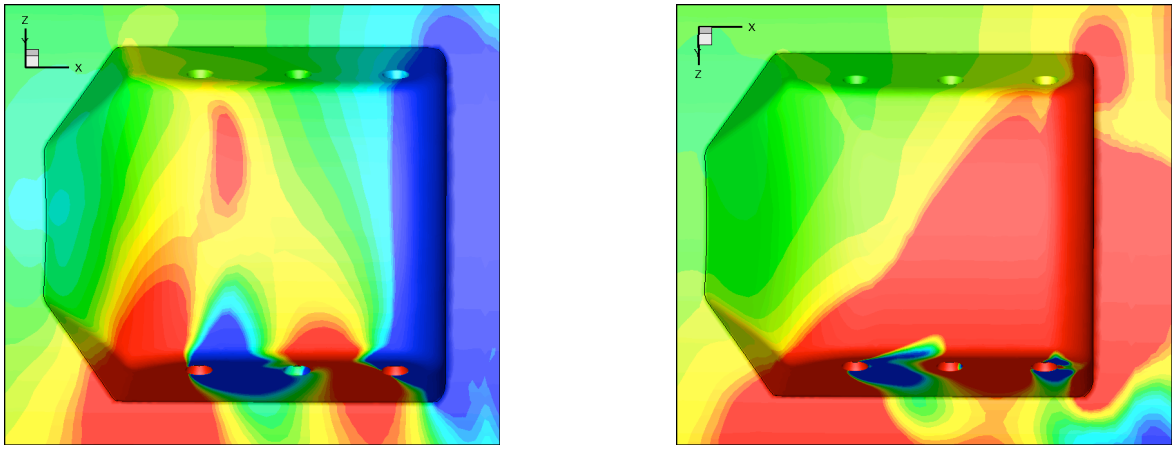

(b) Mach 0.9, E_{J_WV} = 28.27, E_{J_RoCS} = 25.38.

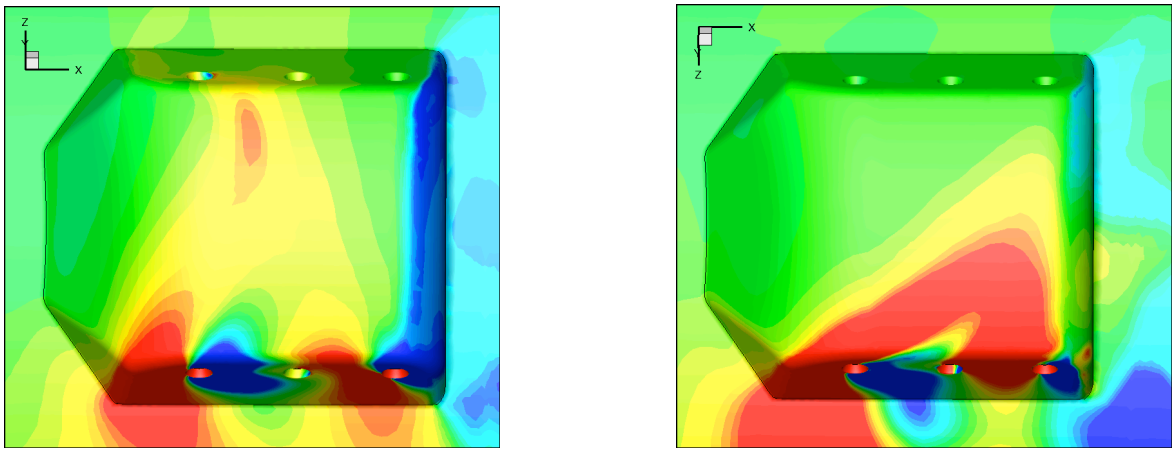

(c) Mach 1.2, E_{J_WV} = 3.34, E_{J_RoCS} = 12.31.

Figure 12. Differential pressure coefficient contours on the RoCS housing, α = 7°, ϕ = 120°, positive roll. Left plot is top RoCS and right plot is bottom RoCS.

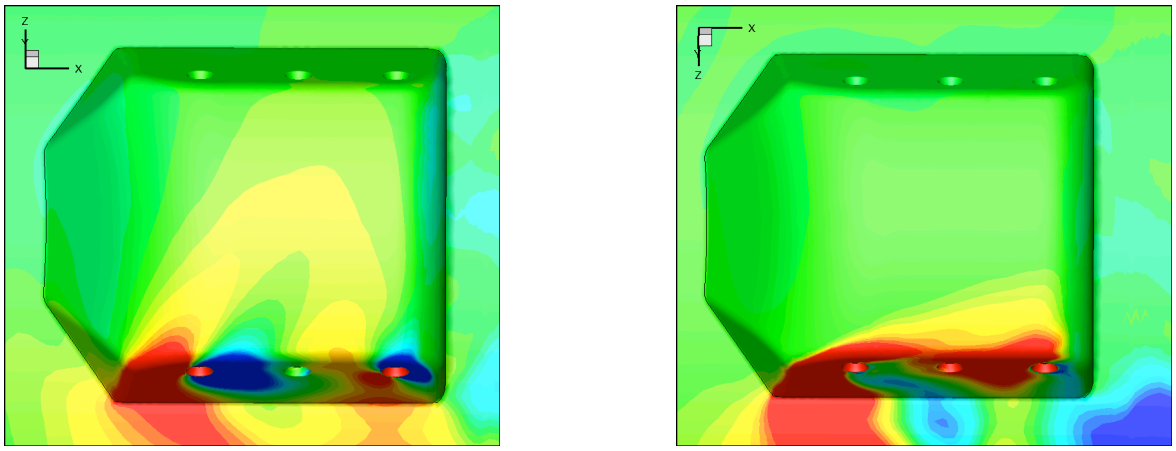

(d) Mach 2, E_{J_WV} = -3.93, E_{J_RoCS} = 14.67.

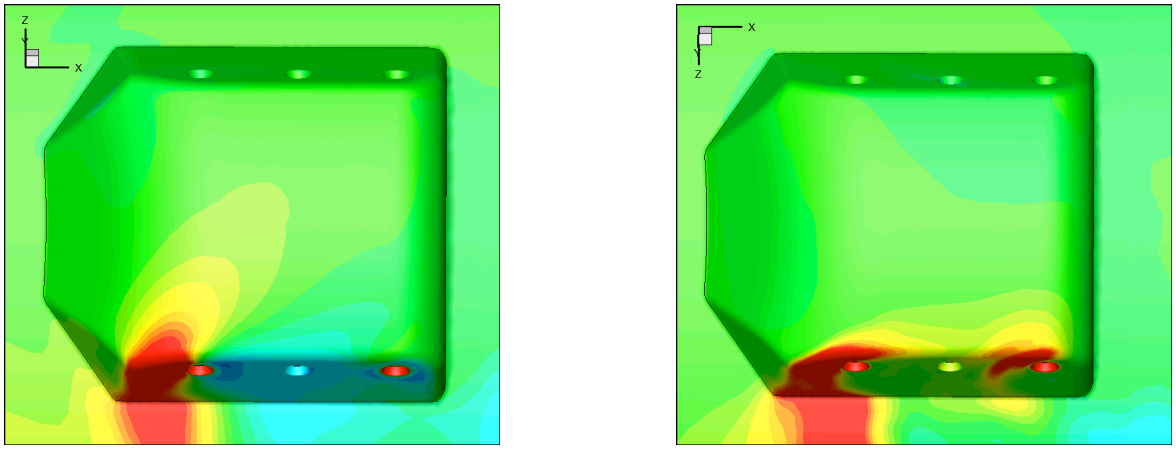

(e) Mach 4, E_{J_WV} = -1.57, E_{J_RoCS} = 3.15.

Figure 12. Concluded.

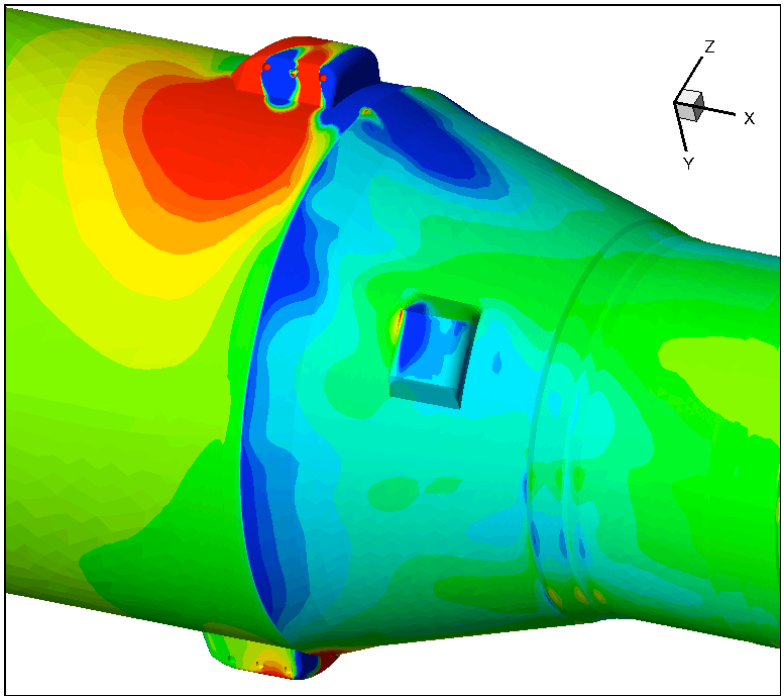

(a) M = 1.0 solution.

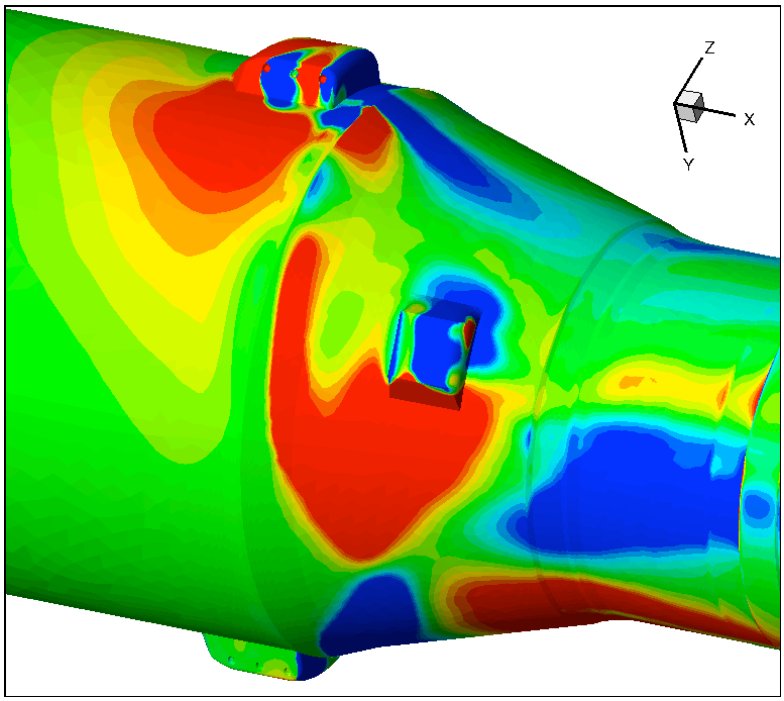

(b) M = 1.2 solution.

Figure 13. Comparison of differential pressure coefficient on the RoCS housing, frustum and BTM for α = 3.5°, ϕ = 120°, and thrusters firing for a positive rolling moment.

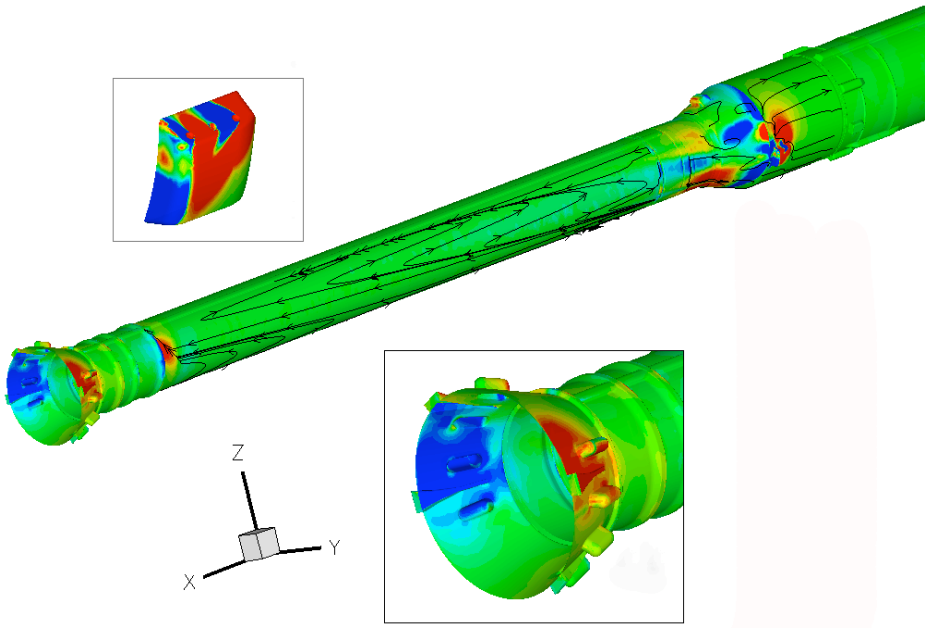

Figure 14. Differential skin friction coefficient vector lines and differential surface pressure coefficient for M = 1.2, α = 3.5°, ϕ = 120°, and thrusters firing for a positive rolling moment.

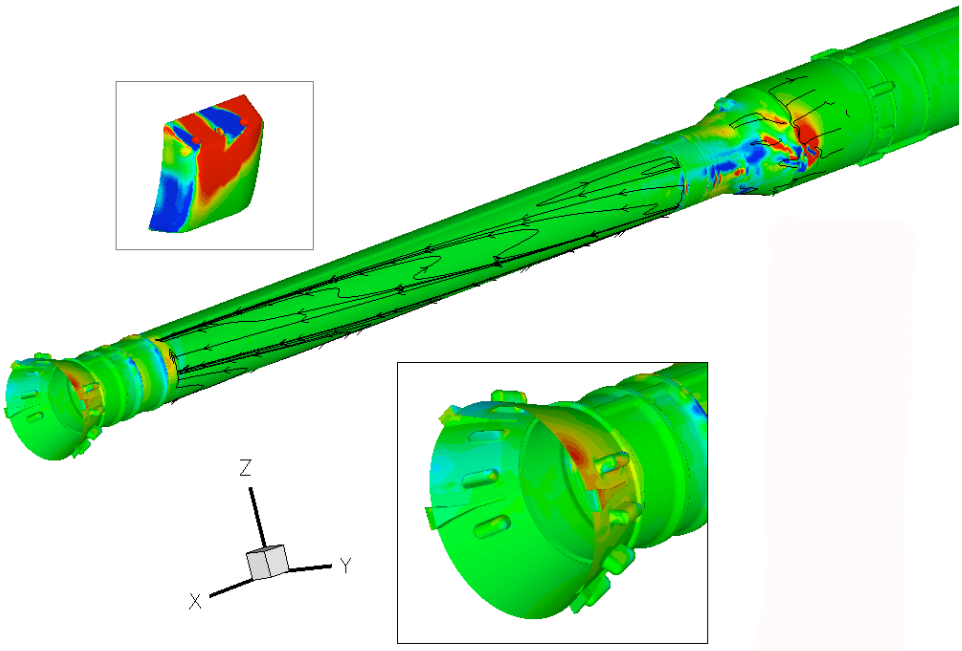

Figure 15. Differential skin friction coefficient vector lines and differential surface pressure coefficient for M = 1.6, α = 3.5°, ϕ = 120°, and thrusters firing for a positive rolling moment.

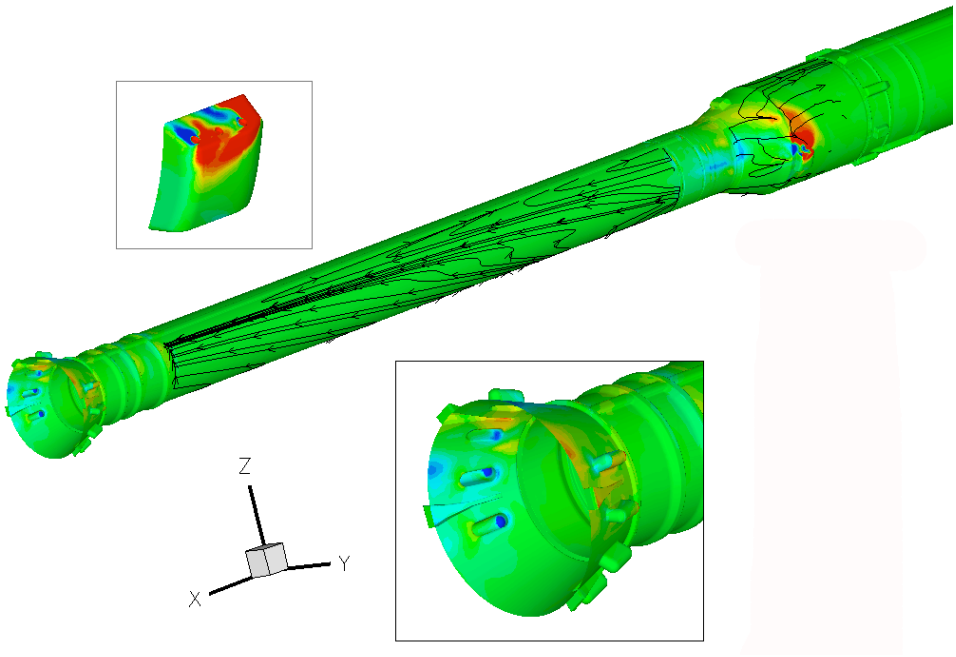

Figure 16. Differential skin friction coefficient vector lines and differential surface pressure coefficient for M = 3, α = 3.5°, ϕ = 120°, and thrusters firing for a positive rolling moment.